

Statistical investigation of structural and transport properties of densely-packed assemblies of overlapping spheres using the resistor network method

Oleg Birkholz^{a,1,*}, Matthias Neumann^{b,1}, Volker Schmidt^b, Marc Kamlah^a

^a*Karlsruhe Institute of Technology, Hermann-von-Helmholtz-Platz 1, 76344
Eggenstein-Leopoldshafen, Germany*

^b*Ulm University, Helmholtzstrasse 18, 89069 Ulm, Germany*

Abstract

Relationships between microstructure characteristics and effective transport properties of granular materials are crucial for many real-world applications. In the present paper microstructure-property relationships of sphere packings are investigated by means of modeling and simulation. Virtual microstructures are generated with the random close packing algorithm. This algorithm provides initial systems of randomly distributed, non-overlapping and densely-packed spheres of a given polydisperse size distribution. Next, the initial sphere packing is further densified until a certain criterion is reached, namely a predefined mean contact angle. In this way, we obtain a large database of slightly overlapping sphere systems. Subsequently, effective transport properties of the sphere systems (solid) and their complementary sets (pores) are determined using the computationally efficient resistor network method. Finally, the generated virtual microstructures are used to establish formulas expressing effective transport properties of sphere packings in terms of the mean contact angle and the standard deviation of the particle radii.

Keywords: Granular material, effective conductivity, resistor network method, sphere packing, microstructure-property relationship, prediction formula

*Corresponding author. Tel.: +49 721 608-24892; Fax: +49 721 608-22347; E-mail address: oleg.birkholz@kit.edu

¹Both authors have equally contributed to the present paper.

1. Introduction

Effective macroscopic properties of heterogeneous media depend strongly on the geometry of their underlying microstructure [1]. In particular, in the case of granular media, the microstructure is of great importance for the overall—so-called effective—transport properties. This means that the effective transport properties may significantly differ from the intrinsic or bulk transport properties of the considered material. The knowledge of effective transport properties in granular materials, such as battery electrodes the active material of which is granular [2, 3], plays a decisive role in many applications. Thus, a better quantitative understanding of relationships between those properties and the corresponding microstructure characteristics can help in the development of improved granular materials.

Relationships between effective transport properties of granular and, in general, porous materials and their microstructure characteristics have been studied for quite some time now. Many formulas have been proposed, expressing effective transport properties in terms of volume fraction of the transporting phase, see [4] for a review. Note that theoretical results for those relationships can only be derived for certain structural scenarios which are hardly representative for real materials [1]. However, in case that it is sufficient to know upper or lower bounds of the effective transport properties, rigorous results are available [5, 1], where the so-called Wiener bounds [6] (anisotropic arrangement of phases) and the Hashin-Shtrikman bounds [7] (isotropic arrangement of phases) are the most prominent ones. These bounds indicate thresholds for the best or the worst effective transport.

If a more precise estimation of effective transport properties is required, usually the effective medium theory (EMT) is used [8]. Especially in the field of cell modeling for lithium-ion batteries, the well-known Bruggeman relation is employed, see for example [9]. This relation is used to estimate the effective transport properties of both the solid and the liquid electrolyte phases inside the electrode structures of the battery. But, as it was pointed out in [9],

the Bruggeman relation, which is used for the ionic transport in the liquid electrolyte, is not applicable to a network of contacting particles. Besides the Bruggeman relation, empirical formulas relating microstructure characteristics to transport properties were derived in [10, 11] using a large database of virtual, but realistic, microstructures which were generated using models from stochastic geometry [12]. Even if these formulas lead to a good fit for a large class of microstructures, deviations are observed when using them for systems of packed spheres as already discussed in Section 5.1 of [11].

As far as the computation of the effective transport properties in the solid phase of contacting spheres is concerned, in [13] a formula was developed which takes the percolation threshold into account. However, the analysis in [13] does not consider polydisperse distributions of particle sizes. Therefore, in the present paper, we focus on the development of empirically fitted prediction formulas which express the effective transport properties of both the solid phase and the pore phase of densely-packed assemblies of overlapping spheres with a polydisperse size distribution by morphological characteristics. The formulas are derived by extensive numerical analysis employing the so-called resistor network (RN) method [14, 15] on virtually generated granular structures.

The rest of this paper is structured as follows. In Section 2, we first recall the RN method sketching the basic idea behind the method. In Section 3, we investigate a series of virtually generated sphere assemblies, calculate their porosities and effective transport properties using the RN method and discuss the results. In the same section, we propose empirically fitted formulas based on numerical simulations to quantify relationships between the microstructure of the sphere systems and the corresponding effective transport properties. Finally, Section 4 summarizes and concludes.

2. Resistor network method

In this section, we recall the RN method for the calculation of effective transport properties of assemblies of spheres. For a more detailed explanation
60 of the method, we refer to [14].

2.1. Conservation law

In the present paper, we consider steady-state transport problems which can be described by the continuity equation

$$\nabla \cdot \vec{F} = 0, \quad (1)$$

where \vec{F} is the flux density vector related to the underlying transport phenomenon. Depending on the specific physical problem, the flux vector can be the heat flux density vector \vec{q} in the case of conservation of energy, the species flux density vector \vec{j} in the case of conservation of species and the current density vector \vec{i} in the case of conservation of charge. Consequently, the constitutive law in Equation (1) becomes either Fourier's, Fick's first or Ohm's law, respectively:

$$\begin{aligned} \vec{q} &= -\boldsymbol{\lambda} \cdot \nabla T, \\ \vec{j} &= -\mathbf{D} \cdot \nabla c, \\ \vec{i} &= -\boldsymbol{\kappa} \cdot \nabla \varphi. \end{aligned} \quad (2)$$

Here, the considered material is represented via the thermal conductivity tensor $\boldsymbol{\lambda}$, the diffusivity tensor \mathbf{D} or the electric conductivity tensor $\boldsymbol{\kappa}$ and the driving forces are the negative gradient of either the temperature T , the concentration
65 c or the electric potential φ , respectively.

For the computation of effective transport properties of transport phenomena fulfilling Equation (1), the RN method can be used independently of the underlying physical problem, see also [16].

2.2. Transport modeling using resistor networks

70 In the following, we show how effective transport properties are modeled in the present paper using resistor networks. Exemplarily, we deal with the effective electric conductivity denoted by κ_{eff} .

In order to calculate effective transport properties by means of the resistor network approach, one has to convert the considered transport phase into an equivalent circuit of resistors. The resulting resistor network consists of nodes and edges representing the resistors between the nodes. If two nodes are connected by an edge, transport can take place between them. This conversion is achieved differently for the solid phase consisting of a system of overlapping spherical particles and the pore phase, *i.e.* the complementary set of the sphere system.

2.2.1. Transport through solid phase

The solid phase is converted into a circuit of resistors as follows. As can be seen in Figure 1, the basis of the resistor network is the transport path through the solid phase depicted by a cluster of spheres connecting the boundaries of the assembly. The nodes are given by the sphere centers and edges are put between two nodes if the corresponding spheres overlap. Moreover, a potential is assigned to each node and weights are assigned to the edges, which define the corresponding resistances. For a pair of nodes I, J , let φ^I and φ^J denote their potentials. If I and J are connected by an edge, the corresponding resistance of this edge, denoted by $R_{\text{solid}}^{I,J}$, is defined by

$$R_{\text{solid}}^{I,J} = \frac{1/\kappa^I + 1/\kappa^J}{4r_c}. \quad (3)$$

Note that $R_{\text{solid}}^{I,J}$ depends only on the respective bulk conductivities of the particles κ^I and κ^J and the contact radius r_c between them, see the right-hand side of Figure 1. In this way, Equation (3) accounts for geometric bottleneck effects.

A system of linear equations is set up, see Equation (6), using the combination of Kirchhoff's law, *i.e.*

$$0 = \mathcal{I}^I = \sum_{J \in \mathcal{N}(I)} \mathcal{I}^{I,J} \quad (4)$$

and Ohm's law, *i.e.*

$$\mathcal{I}^{I,J} = \frac{\varphi^I - \varphi^J}{R_{\text{solid}}^{I,J}}. \quad (5)$$

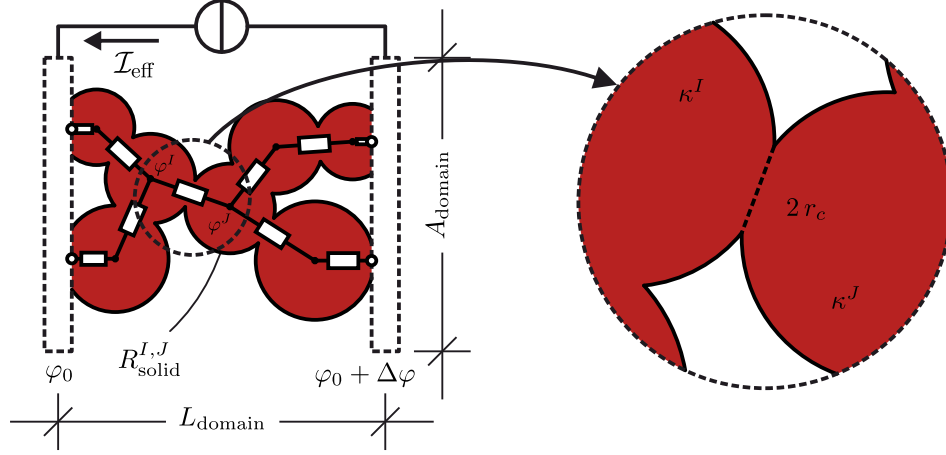


Figure 1: 2D sketch of a single resistance between two overlapping spheres inside a network of overlapping spheres.

Here $\mathcal{N}(I)$ denotes the set of neighbors of I . Moreover, \mathcal{I}^I denotes the electric current at node I and $\mathcal{I}^{I,J}$ denotes the electric current from I to J . Thus, at every node I the sum of the electric current is

$$\mathcal{I}^I = \sum_{J \in \mathcal{N}(I)} \frac{\varphi^I - \varphi^J}{R_{\text{solid}}^{I,J}} = 0. \quad (6)$$

Due to the applied potential drop of $\Delta\varphi$ around a reference potential φ_0 at the boundary nodes, the system of linear equations given in Equation (6) can be solved for all potentials φ^I . Finally, the effective current \mathcal{I}_{eff} can be evaluated as the sum of all currents entering or leaving the boundary nodes and the effective electric conductivity is given by

$$\kappa_{\text{eff}} = \frac{\mathcal{I}_{\text{eff}} L_{\text{domain}}}{\Delta\varphi A_{\text{domain}}}, \quad (7)$$

85 where L_{domain} and A_{domain} is the domain length and cross section area, respectively.

2.2.2. Transport through pore phase

Concerning the pore phase, the conversion into an equivalent circuit of resistors involves the so-called Laguerre tessellation or generalized Voronoi tessellation [17], see Figure 2. To be more precise, we consider the Laguerre tessellation, where the generators are given by the midpoints of the particles and their weights are given by the corresponding radii. For detailed information regarding the Laguerre tessellation of sphere packings, we refer to [18]. The computation is done by employing the software library Voro++ [19]. By means of the Laguerre tessellation we are able to decompose the pore phase by so-called Laguerre cells such that—roughly speaking—the Laguerre cell corresponding to a given spherical particle represents all points of the pore phase around this particle.²

Having computed the Laguerre tessellation, the nodes of the resistor network are given by the vertices of the Laguerre cells, *i.e.* by its 0-dimensional facets. The nodes are interpreted as the pore centers of the corresponding pore network. Furthermore, the 1-dimensional facets of the Laguerre tessellation, which can be interpreted as the medium axes of the interconnecting pores, form the edges, *i.e.* the pore throats, between the nodes. Similar to the case of the solid phase, a potential φ^I is associated with each node I and pore throat resistances $R_{\text{pore}}^{I,J}$ are assigned to the edges between I and J for all connected nodes, see Figure 2.

For a given pair of connected nodes I and J , the pore throat resistance $R_{\text{pore}}^{I,J}$ is calculated in three steps. As a first step, the geometry of an individual pore throat is defined by decomposing the surrounding region of the corresponding edge into compartments. In case of 2D, the compartments are constructed as the areas which are given by triangles defined by the nodes of the considered

²Note that for general systems of overlapping spheres, the Laguerre cell corresponding to a given particle might be empty [17]. This property depends on the degree of pairwise overlapping between the particles [18]. In our case, where the particles are only slightly overlapping, each spherical particle generates a non-empty Laguerre cell.

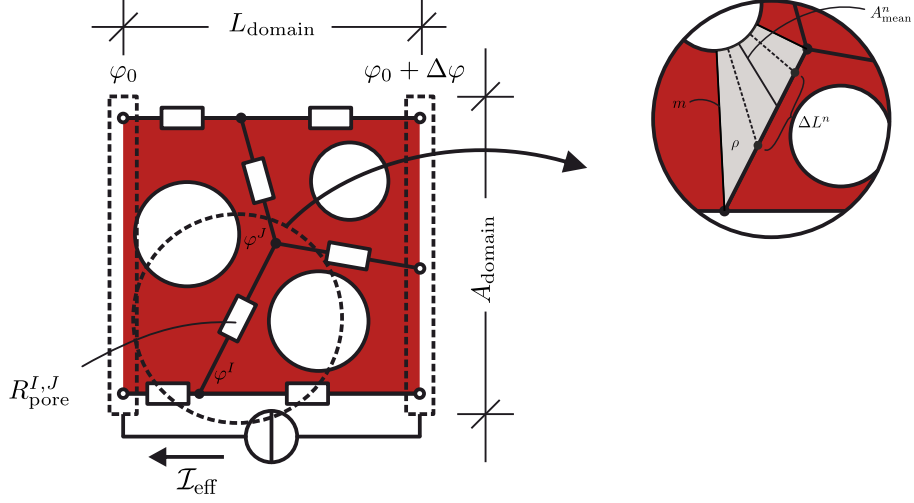


Figure 2: 2D sketch of resistances of a pore throat inside a pore network.

edge and the associated sphere centers, where the intersection area with the associated spheres is subtracted from. In the 3D case, the surrounding region
 115 is the volume given by tetrahedrons, which, as an extension of the 2D case, are additionally defined by the centers of the faces, *i.e.* 2-dimensional facets, of the Laguerre cells which meet at the considered edge. The intersecting volumes of the associated spheres are then subtracted from the tetrahedrons.³

In a second step, based on this decomposition, the considered individual pore throat is divided into sub-throats, see the gray-shaded area on the right-hand side of Figure 2 for the 2D case, and the grey-shaded volume in Figure 3 for the 3D case. The resistance $R_m^{I,J}$ of a sub-throat m of the edge between I and J is

³Formally, the surrounding region is defined by the set $\mathcal{T} \setminus \mathcal{S}$. Here \mathcal{S} denotes the associated spheres, while \mathcal{T} is defined as the convex hull of the edge defining nodes, the associated sphere centers and the centers of the 2-dimensional facets which meet at the considered edge and which belong to the Laguerre cell corresponding to the associated sphere.

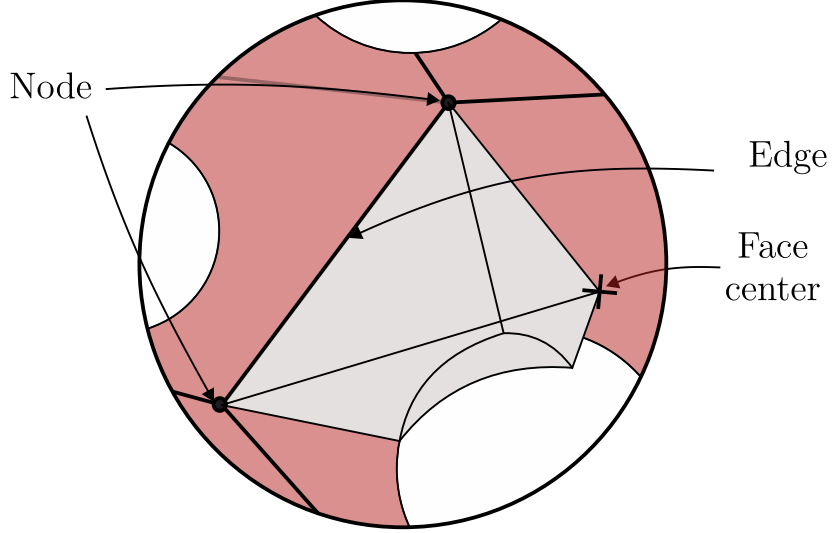


Figure 3: 3D sketch of a throat construction in a pore network. The grey-shaded volume represents a sub-throat.

calculated as the sum of wire resistances. For this purpose, we further subdivide the sub-throat m into a wire of n_{incr} parts, called increments, and obtain

$$R_m^{I,J} = \sum_{n=1}^{n_{\text{incr}}} \Delta R_m^n = \rho \sum_{n=1}^{n_{\text{incr}}} \frac{\Delta L^n}{A_{\text{mean}}^n}, \quad (8)$$

where ρ is the bulk resistivity and ΔR_m^n is the resistance of the n 'th increment. Moreover, ΔL^n is the length and A_{mean}^n is the mean length of the line which has to be passed in the 2D case and the mean cross section area of the n 'th increment in the 3D case. Note that in Figure 2, n_{incr} is equal to 3. The number of increments n_{incr} is successively increased and thereby the size of ΔL^n is successively reduced until the resulting resistance of the sub-throat in Equation (8) does not significantly change by a further increase of n_{incr} . To be precise, the iteration is stopped in case that a further increase of n_{incr} leads to change of the corresponding resistance by less than 5%.

Finally, in the third step, the resistance $R_{\text{pore}}^{I,J}$ of the individual pore throat between I and J is calculated as a parallel connection of the m_{sthr} sub-throat resistances $R_m^{I,J}$ as

$$R_{\text{pore}}^{I,J} = \left(\sum_{m=1}^{m_{\text{sthr}}} \frac{1}{R_m^{I,J}} \right)^{-1}. \quad (9)$$

Similar to the case of the solid phase considered in Section 2.2.1 the combination of Kirchoff’s and Ohm’s law is used to set up a system of linear equations. Imposing a potential drop $\Delta\varphi$ around a reference potential φ_0 at the boundary nodes, the system of linear equations is solved for the effective electric current. Then, the effective conductivity is obtained using Equation (7).

Summarizing, we have presented the RN method to compute effective transport properties for overlapping sphere assemblies and the corresponding complementary phase considered as solid phase and pore phase of a granular material, respectively. A validation of this method can be found in [14]. In the following we apply the RN method to investigate quantitative microstructure-property relationships for assemblies of overlapping spheres with a polydisperse size distribution.

3. Effective transport properties

In this section, we use the RN method to compute effective transport parameters for assemblies of overlapping spheres with a polydisperse size distribution. We first explain how the assemblies were created. Then, we empirically derive formulas quantifying the influence of the morphology of those sphere systems on their effective transport properties. Finally, the results are evaluated and discussed.

3.1. Generation of virtual random sphere assemblies

The virtual sphere assemblies were generated as follows. First, an initial assembly of non-overlapping spheres was generated using the random close packing algorithm (RCP) [20] in a cubic sampling window. Generally, the RCP delivers

a randomly distributed, densely packed and overlap-free assembly of monosized spheres. However, following [21], the basic RCP was extended to account for more general size distributions of spheres. In the present paper, we use a discrete radius distribution which can take five different radii $r_1, \dots, r_5 > 0$ such that the probability of a sphere radius being r_i is given by $q_i = \mathbb{P}(X \in A_i) / \mathbb{P}(\cup_{i=1}^5 A_i)$, where X is a normally distributed random variable with mean $r_{\text{mean}} > 0$ and standard deviation $r_\sigma > 0$ and A_1, \dots, A_5 are disjoint intervals on the positive real line depending on r_{mean} and r_σ .⁴ In doing so, we generated virtual granular materials, which consisted of five types of particles with different sizes.

In a further step, in order to establish conducting pathways through overlapping spheres, the initial sphere packings were further densified. To this end, we used an algorithm which we call numerical sintering and which is similar to the procedure used in [22, 23]. In our case, while isotropically and successively reducing the cubic sampling window, the spheres are pushed towards each other until a certain degree of densification is reached. In the present paper, we used the mean contact angle θ_{mean} to represent the degree of densification, where θ_{mean} is defined as the mean of all contact angles of an assembly. An individual contact angle for a pair of overlapping spheres is the maximum of the two angles enclosing the contact radius of the two spheres. In order to avoid ordering effects due to the presence of a flat wall, periodic boundary conditions were applied.

We generated 100 different scenarios of randomly distributed and densely packed sphere assemblies, where in each scenario the values of the model parameters r_σ and θ_{mean} were chosen at random. The parameter r_σ was chosen uniformly at random between 0 and 0.25 length units (lu) representing monosized up to highly polydisperse size distributions. The parameter θ_{mean} is chosen uniformly at random between 0.05° and 30° resembling barely and highly overlapping sphere packings, respectively. The mean particle radius $r_{\text{mean}} = 1$ lu is

⁴To be precise, we choose $A_1 = (r_{\text{mean}} - 3r_\sigma, r_{\text{mean}} - 9r_\sigma/5]$, $A_2 = (r_{\text{mean}} - 9r_\sigma/5, r_{\text{mean}} - 3r_\sigma/5]$, $A_3 = (r_{\text{mean}} - 3r_\sigma/5, r_{\text{mean}} + 3r_\sigma/5]$, $A_4 = (r_{\text{mean}} + 3r_\sigma/5, r_{\text{mean}} + 9r_\sigma/5]$ and $A_5 = (r_{\text{mean}} + 9r_\sigma/5, r_{\text{mean}} + 3r_\sigma]$.

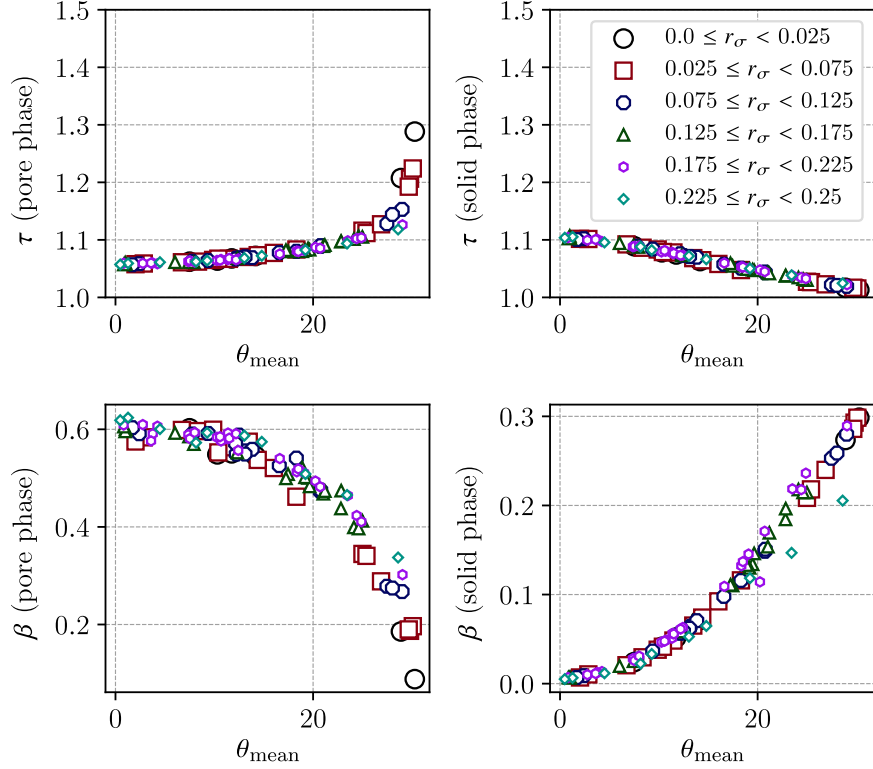


Figure 4: Mean geodesic tortuosity τ (top) and constrictivity β (bottom) over θ_{mean} , where different ranges of r_σ are highlighted with different colors. The results are shown for the pore phase (left) and the solid phase (right).

fixed for all cases. In order to obtain sphere systems which are representative with respect to their effective transport properties, the number of spheres in each generated assembly was chosen to be 5000.

3.2. Prediction of effective conductivity

3.2.1. The role of tortuosity and constrictivity

Based on the 100 scenarios described in Section 3.1 we investigated the relationship between the model parameters r_σ and θ_{mean} and the microstructure characteristics mean geodesic tortuosity τ and constrictivity β of the solid and

the pore phase, respectively. See [24] for the formal mathematical definition of τ and β . These parameters are of central importance for effective transport properties such as effective conductivity or permeability.⁵ Note that in a previous study [11], where we used three different stochastic microstructure models to simulate more than 8000 virtual porous microstructures, the parametric prediction formula

$$\widehat{M}_0 = \frac{\phi^{1.67-0.48\beta}}{\tau^{5.18}} \quad (10)$$

was empirically derived for the so-called M -factor $M = \kappa_{\text{eff}}/\kappa_{\text{bulk}}$, which is the ratio of effective over bulk conductivity. Here ϕ denotes the volume fraction of the conducting phase, τ its mean geodesic tortuosity and β its constrictivity.

While τ measures the windedness of shortest transportation paths, β is a descriptor for bottleneck effects of the transporting phase. If $\beta = 1$, there are no bottlenecks at all and the closer β is to 0, the stronger the effect of bottlenecks [24]. In Figure 4, τ and β are drawn as functions of θ_{mean} for both the solid and the pore phases of the sphere systems considered in the present paper. Different ranges of r_σ are indicated by different colors and symbols. One can observe that the mean contact angle strongly influences the microstructure characteristics mean geodesic tortuosity τ and constrictivity β of the pore and solid phase, whereas the dependence of τ and β on r_σ is much less pronounced. The dependence of τ and β on the parameters θ_{mean} and r_σ of the sphere packing suggests that effective transport parameters of the microstructures based on the sphere packings considered in the present paper can be expressed in terms of r_σ and θ_{mean} . Therefore, in addition to the prediction formula (10), we empirically derive further prediction formulas which quantify the relationship between r_σ and θ_{mean} one the one hand and the considered effective transport parameters on the other hand.

⁵For the computation of τ and β , the virtual sphere assemblies were discretized on a cubic grid with a grid size of 1/30 lu.

3.2.2. Expressing porosity by model parameters

For each virtual sphere assembly considered in Section 3.1, the effective transport properties for both the solid and the pore phases were calculated using the RN method described in Section 2. In the following, charge transport was considered as a representative of the transport phenomena mentioned in Section 2, where we consider effective electric conductivity κ_{eff} as the transport property of interest. In particular, similar to the investigations described in Section 3.2.1, we evaluate the dimensionless ratio $M = \kappa_{\text{eff}}/\kappa_{\text{bulk}}$, where κ_{bulk} is the bulk conductivity of the material. In the following, we call M the effective transport parameter.

Figure 5a shows the dependency of the porosity ϕ_{pore} on the model parameters θ_{mean} and r_{σ} . We observe that the porosity is decreasing with increasing values of θ_{mean} . This effect is not surprising since the higher the value of θ_{mean} the stronger is the degree of densification during the numerical sintering. Moreover, a slight increase of porosity is observed if r_{σ} is increasing. Based on our simulated data, we found that the porosity can be expressed as a function of θ_{mean} and r_{σ} by

$$\hat{\phi}_{\text{pore}} = \frac{b_0}{b_1 - \exp^{b_2 \theta_{\text{mean}} - b_3 r_{\sigma}}}, \quad (11)$$

which nicely approximates the porosity ϕ_{pore} of the sphere assemblies, where $b_0 = -15.625$, $b_1 = -43.277$, $b_2 = 0.166$ and $b_3 = 1.334$ were determined by means of the least-squares method. Note that the mean absolute percentage error (MAPE) of the prediction formula given in Equation (11) is relatively low being equal to 3.17 %.

3.2.3. Predicting effective transport parameters

In Figure 5b, the effective transport parameter of the solid phase M_{solid} is considered. One can observe that this quantity also depends on θ_{mean} and r_{σ} . For instance, if r_{σ} reaches the lowest and θ_{mean} the largest value, then the effective transport parameter $M_{\text{solid}}^{\text{RN}}$ is at its maximum, where the superscript RN means that this quantity is computed by means of the resistor network method

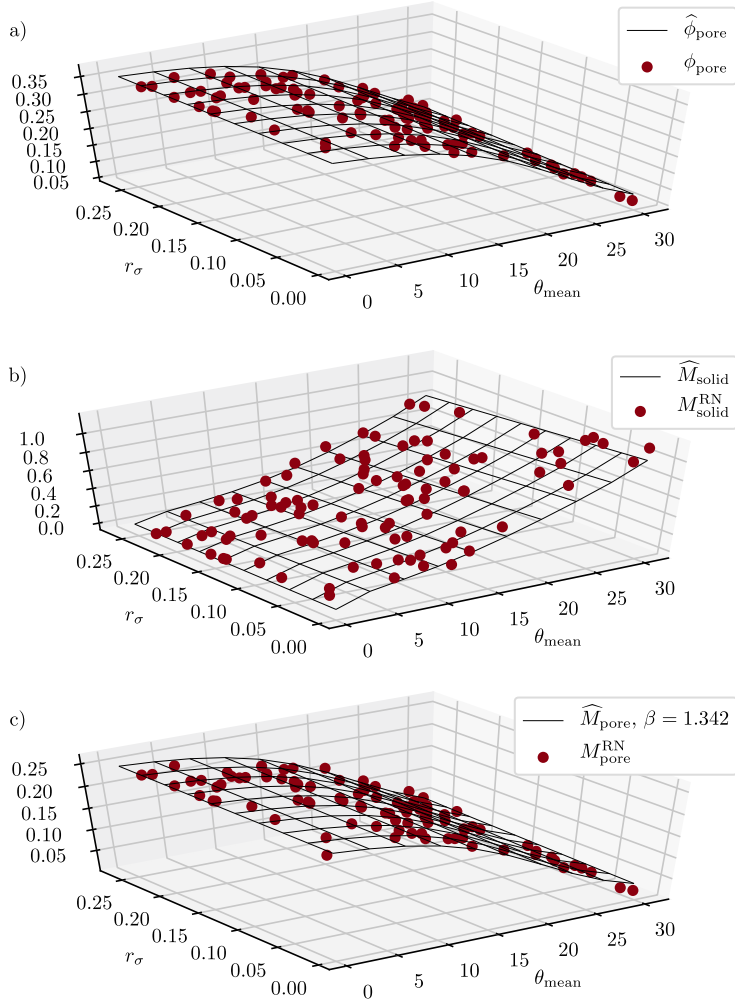


Figure 5: Influence of sphere packing parameters θ_{mean} and r_σ on porosity a), effective transport through the solid phase b), and effective transport through the pore phase c). The red points indicate the results obtained by the RN method, while the black curves indicate the results obtained from the parametric prediction formulas given in Equations (11), (12), and (13), respectively.

explained in Section 2. It is interesting to note that the influence of r_σ on $M_{\text{solid}}^{\text{RN}}$ becomes smaller if the degree of densification decreases, *i.e.*, θ_{mean} approaches zero. More precisely, this means that the effective transport parameter does not significantly change along r_σ provided that θ_{mean} is close to 0. In this case, the reducing contact area between particles induced by the low values of θ_{mean} clearly dominates the effective transport parameter $M_{\text{solid}}^{\text{RN}}$. Note that for cases of very large θ_{mean} and very low r_σ the effective transport parameter $M_{\text{solid}}^{\text{RN}}$ can be larger than 1. As was pointed out in Section 2, in the framework of the RN method for the solid phase, a vital part is the correct computation of the resistances of individual contact pairs. Obviously, for extreme cases, if the porosity ϕ_{pore} approaches zero and, vice versa, if the packing factor $\phi_{\text{solid}} = 1 - \phi_{\text{pore}}$ is close to 1, the contact areas between the spheres are likely to overlap each other. As for the present paper, the calculation of individual contact pair resistances is based on the geometric bottleneck effect of a single contact pair and does not account for the influence of neighboring contact pairs. In other words, in cases of large contact angles and, additionally, low porosity, overlapping contact areas between contact pairs seem to lead to an overestimation of the effective transport parameters provided by the RN method. On the one hand, this shows the limits of the RN method considering solid phase transport, on the other hand, we argue that in cases of porosities close to zero, the use of RN method needs further adjustments. From literature, values of θ_{mean} between 0° and 30° [25] and packing factors below 90 % [15] seem to be preferred regarding the RN method as presented here.

We found that the relationship between the effective transport parameter of the solid phase $M_{\text{solid}}^{\text{RN}}$ and the model parameters θ_{mean} and r_σ can be appropriately described by the quantity

$$\widehat{M}_{\text{solid}} = (\phi_{\text{solid}} - \phi_{\text{solid,c}})^{a_0 + \frac{a_1}{\theta_{\text{mean}}}} + \frac{a_2}{a_3 - \theta_{\text{mean}}} + a_4 r_\sigma, \quad (12)$$

where $a_0 = 0.8015$, $a_1 = 0.3227$, $a_2 = -13.88$, $a_3 = 47.37$ and $a_4 = 0.5284$ were determined by means of the least-square method. Note that $\phi_{\text{solid}} = 1 - \phi_{\text{pore}}$ is the volume fraction of the solid phase, *i.e.* packing factor, and $\phi_{\text{solid,c}}$ is

the percolation threshold which is estimated from the simulation results to be
 250 equal to 0.62. The mean absolute percentage error of the prediction formula
 given in Equation (12) is 24.91 % which still is reasonably low. Regarding the
 overestimation of the RN method for high values of θ_{mean} and ϕ_{solid} , it can be
 seen in Figure 5b that in the given range the prediction formula (12) does not
 exceed the theoretical threshold of 1.

Finally, in Figure 5c, the effective transport parameter of the pore phase
 M_{pore} is focused. The influence of r_{σ} seems to be even less pronounced than for
 the solid phase. Besides that, the qualitative behavior of $M_{\text{pore}}^{\text{RN}}$ in dependence
 of θ_{mean} and r_{σ} is rather similar to the one of porosity shown in Figure 5a.
 Moreover, it turns out that the simple Bruggeman relation [26, 27] yields a
 good agreement with the numerical results if the coefficient β_{brugg} is suitably
 fitted. From our simulation results, the quantity

$$\widehat{M}_{\text{pore}} = \left(\widehat{\phi}_{\text{pore}} \right)^{\beta_{\text{brugg}}} \quad (13)$$

255 delivers a good approximation of the effective transport parameter $M_{\text{pore}}^{\text{RN}}$ com-
 puted using the RN method, where $\beta_{\text{brugg}} = 1.342$ was determined by the
 least-square method. This leads to a MAPE of 13.64 %. Note that for the
 porosity, we plug in the quantity $\widehat{\phi}_{\text{pore}}$ from Equation (11).

3.3. Discussion of prediction formulas

260 Note that the prediction formulas given in Equations (12) and (13) lead to a
 significantly better fit for the sphere assemblies considered in the present paper
 than Equation (10) of [11] which predicts the effective transport parameters by
 means of their mean geodesic tortuosity and constrictivity, see Figure 6. This is
 not surprising since Equation (10) has been derived for virtual microstructures
 265 exhibiting a rather different morphology than the sphere assemblies considered
 in the present paper. Furthermore, limitations of Equation (10) for microstruc-
 tures arising from systems of slightly overlapping spheres haven been already
 discussed in Section 5.1 of [11]. Note that one reason for the large error regard-
 ing the prediction of the M -factor of the solid phase of sphere assemblies can

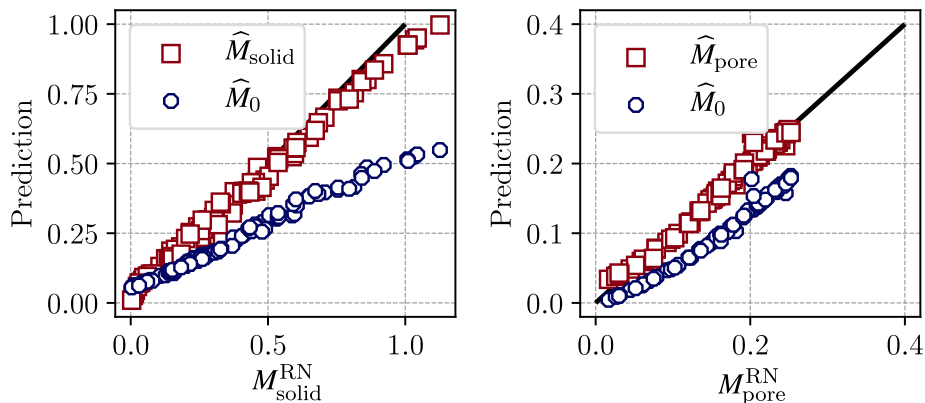


Figure 6: Visualization of the goodness-of-fit of the predictors $\widehat{M}_{\text{solid}}$ and $\widehat{M}_{\text{pore}}$ given in Equations (12) and (13) for sphere assemblies compared to the predictor \widehat{M}_0 given in Equation (10).

270 be explained by the fact that Equation (10) was derived for virtual microstructures which are percolating even for low volume fractions of the conducting phase. In other words, in contrast to Equation (12), the percolation threshold of the sphere assemblies considered in the present paper is not captured in Equation (10). This leads to an overestimation for low values of M_{solid} .
 275 Vice versa, the prediction formulas given in Equations (12) and (13) express effective transport properties by means of the parameters θ_{mean} and r_{σ} , which are only well defined for assemblies of slightly overlapping spherical particles. Thus those prediction formulas are restricted to materials, the microstructure of which consists of an assembly of slightly overlapping spherical particles.

280 4. Summary and Conclusion

In the present paper, we combined the generation of virtual sphere packings with the RN method to study relationships between the morphology of sphere assemblies with polydisperse size-distributions and their effective transport properties. In particular, we focused on the dispersity of the particle size
 285 distribution and the degree of overlap between the spheres.

For this purpose, we created 100 different assemblies of 5000 spherical particles by means of a random close packing algorithm. The assemblies were densified using a simple numerical sintering algorithm. The generated structures differed with respect to the degree of polydispersity, *i.e.*, the parameter r_σ determining the standard deviation of the spheres' radii, and with respect
290 to the degree of densification, *i.e.*, the mean contact angle θ_{mean} between the spheres. It was shown that both, geometrical microstructure characteristics and effective transport properties depend on the model parameters r_σ and θ_{mean} .

On the one hand, concerning porosity ϕ_{pore} and the effective transport parameter of the solid phase M_{solid} , we empirically derived parametric prediction
295 formulas expressing those quantities by θ_{mean} and r_σ . On the other hand, for the considered sphere packings, the well-known Bruggeman relation leads to good estimation of the effective transport parameter of the pore phase M_{pore} . In this case, we can use the derived expression for porosity in terms of θ_{mean}
300 and r_σ to obtain relationships between the latter model parameters and the effective transport parameter of the pore phase M_{pore} . The obtained results lead to a better understanding of microstructural influence on transport phenomena of sphere assemblies, which can be used for tailoring microstructures with enhanced transport properties.

305 **Acknowledgements**

This work has been funded by the German Federal Ministry for Economic Affairs and Energy (BMWi) granted through Project Management Jülich (03ET6095A and 03ET6095E). Furthermore, this work contributes to the research performed at CELEST (Center for Electrochemical Energy Storage Ulm-Karlsruhe). Finally, we would like to acknowledge the cooperation with the Graduate School
310 SiMET - Simulation of Mechanical, Electrical and Thermal effects in Li-ion batteries (281041241/GRK2218).

References

- [1] S. Torquato, *Random Heterogeneous Materials: Microstructure and Macroscopic Properties*, Springer, New York, 2002.
- [2] M. Neumann, N. Bohn, A. Wagner, M. Osenberg, A. Hilger, I. Manke, J. Binder, V. Schmidt, Characterization of hierarchically structured electrodes with different thicknesses by means of experiments and image analysis., *Materials Characterization* 155 (2019) 109778.
- [3] S. Wu, B. Yu, Z. Wu, S. Fang, B. Shi, J. Yang, Effect of particle size distribution on the electrochemical performance of micro-sized silicon-based negative materials, *RSC Advances* 8 (2018) 8544–8551.
- [4] L. Shen, Z. Chen, Critical review of the impact of tortuosity on diffusion, *Chemical Engineering Science* 62 (2007) 3748–3755.
- [5] D. Jeulin, *Spatial statistics and micromechanics of materials*, in: K. Mecke, D. Stoyan (Eds.), *Morphology of Condensed Matter*, Springer, Berlin, 2002, pp. 3–36.
- [6] G. C. J. Bart, *Thermal conduction in con-homogeneous and phase change media*, Ph.D. thesis, TU Delft (1994).
- [7] Z. Hashin, S. Shtrikman, A variational approach to the theory of the effective magnetic permeability of multiphase materials, *Journal of Applied Physics* 33 (1962) 3125–3131.
- [8] R. Landauer, The electrical resistance of binary metallic mixtures, *Journal of Applied Physics* 23 (1952) 779–784.
- [9] T. R. Ferguson, M. Z. Bazant, Nonequilibrium thermodynamics of porous electrodes, *Journal of The Electrochemical Society* 159 (2012) A1967–A1985.

- [10] O. Stenzel, O. M. Pecho, L. Holzer, M. Neumann, V. Schmidt, Predicting effective conductivities based on geometric microstructure characteristics, AICHE Journal 62 (2016) 1834–1843.
- [11] M. Neumann, O. Stenzel, F. Willot, L. Holzer, V. Schmidt, Quantifying the influence of microstructure on effective conductivity and permeability: virtual materials testing., International Journal of Solid and Structures 184 (2020) 211–220.
- [12] S. N. Chiu, D. Stoyan, W. S. Kendall, J. Mecke, Stochastic Geometry and its Applications, 3rd Edition, J. Wiley & Sons, Chichester, 2013.
- [13] C. Argento, D. Bouvard, Modeling the effective thermal conductivity of random packing of spheres through densification, International Journal of Heat and Mass Transfer 39 (1996) 1343–1350.
- [14] O. Birkholz, Y. Gan, M. Kamlah, Modeling the effective conductivity of the solid and the pore phase in granular materials using resistor networks, Powder Technology 351 (2019) 54–65.
- [15] J. Ott, B. Völker, Y. Gan, R. M. McMeeking, M. Kamlah, A micromechanical model for effective conductivity in granular electrode structures, Acta Mechanica Sinica 29 (2013) 682–698.
- [16] T. C. Choy, Effective Medium Theory: Principles and Applications, 2nd Edition, Oxford University Press, Oxford, 2015.
- [17] F. Aurenhammer, Power diagrams: properties, algorithms and applications, SIAM Journal on Computing 16 (1987) 78–96.
- [18] C. Redenbach, Microstructure models for cellular materials, Computational Materials Science 44 (2009) 1397–1407.
- [19] C. Rycroft, Voro++: a three-dimensional Voronoi cell library in C++.
- [20] W. S. Jodrey, E. M. Tory, Computer simulation of close random packing of equal spheres, Physical Review A 32 (1985) 2347–2351.

- 365 [21] Y. Gan, M. Kamlah, J. Reimann, Computer simulation of packing structure in pebble beds, *Fusion Engineering and Design* 85 (2010) 1782–1787.
- [22] J. K. Ott, B. Völker, Y. Gan, R. M. McMeeking, M. Kamlah, A micromechanical model for effective conductivity in granular electrode structures, *Acta Mechanica Sinica* 29 (2013) 682–698.
- 370 [23] J. K. Ott, Modeling the microstructural and micromechanical influence on effective properties of granular electrode structures with regard to solid oxide fuel cells and lithium ion batteries, PhD thesis, Karlsruhe Institute of Technology (2015).
- [24] M. Neumann, C. Hirsch, J. Staněk, V. Beneš, V. Schmidt, Estimation of geodesic tortuosity and constrictivity in stationary random closed sets, 375 *Scandinavian Journal of Statistics* 46 (2019) 848–884.
- [25] J. Sanyal, G. M. Goldin, H. Zhu, R. J. Kee, A particle-based model for predicting the effective conductivities of composite electrodes, *Journal of Power Sources* 195 (19) (2010) 6671–6679.
- 380 [26] D. A. G. Bruggeman, Berechnung verschiedener physikalischer Konstanten von heterogenen Substanzen. I. Dielektrizitätskonstanten und Leitfähigkeiten der Mischkörper aus isotropen Substanzen, *Annalen der Physik* 416 (1935) 636–664.
- [27] B. Tjaden, S. J. Cooper, D. J. L. Brett, D. Kramer, P. R. Shearing, On the 385 origin and application of the Bruggeman correlation for analysing transport phenomena in electrochemical systems, *Current Opinion in Chemical Engineering* 12 (2016) 44–51.